Difference in driver gene expression patterns between perihilar and peripheral intrahepatic cholangiocarcinoma in an experimental mouse model.

Toshiyuki Adachi[1], Tomohiko Adachi[1], Takehiro Nakagaki[2], Shinichiro Ono[1], Masaaki Hidaka[1], Shinichiro Ito[1], Kengo Kanetaka[1], Mitsuhisa Takatsuki[1], Noriyuki Nishida[2], Susumu Eguchi[1]*

[1] Department of Surgery, Graduate School of Biomedical Sciences, Nagasaki University, Nagasaki, Japan

[2] Department of. Molecular Microbiology and Immunology. Nagasaki University Graduate School of Biomedical Sciences, Nagasaki, Japan

* Corresponding author. Tel.: +81-95-8197316; Fax: +81-95-8197319; Email: sueguchi@nagasaki-u.ac.jp

Word count: 3,343

Number of tables and figures: 0 tables, 5 figures

Keywords: intrahepatic cholangiocarcinoma, driver gene analysis, carcinogenesis, mice model, epithelial-mesenchymal transition

Abstract

Background: The prognosis of intrahepatic cholangiocarcinoma (ICC) is based on tumor localization; however, the mechanism remains unknown. Therefore, we investigated the biological characteristics of perihilar and peripheral ICC in a mouse model.

Methods: The model was established by the administration of three oncogenic plasmids harboring myristoylated AKT, mutated human YAP, and pCMV-Sleeping Beauty into the mice. The perihilar and peripheral ICC tumors that developed in the same mouse were assessed for the expression of cell adhesion factors and driver genes with immunohistochemistry and reverse transcription polymerase chain reaction (RT-PCR).

Results: The perihilar ICC tumors were irregularly shaped, whereas the peripheral tumors were mostly circular, similar to the differences found in patients. Alpha-smooth muscle actin was strongly expressed in the perihilar tumors at 10 weeks, and vimentin expression was significantly up-regulated in the perihilar ICC at 14 weeks. *Fgfr2* level significantly increased in peripheral ICC at 10 weeks, whereas *Idh2* expression was up-regulated in perihilar ICC.

Conclusions: Despite of diffuse injection of oncogenic plasmid, expression of driver genes and oncogenes in ICC tumor cells differs depending on the tumor localization, resulting in changes in epithelial-mesenchymal transition, which may explain the different

outcomes of patients with peripheral and perihilar ICC.

Abbreviations

ICC: intrahepatic cholangiocarcinoma

RT-PCR: reverse transcription polymerase chain reaction

EMT: epithelial-mesenchymal transition

HE: hematoxylin and eosin

CK: cytokeratin

A-SMA: α-smooth muscle actin

NCAM: neural cell adhesion molecule

SDS: sodium dodecyl sulfate

Introduction

ICC accounts for 5% of all primary liver cancers in Japan [1]. Radical surgical resection has been the only main treatment for ICC with favorable results and is like that adopted for hepatocellular carcinoma. However, the recurrence rate reaches up to 50 - 80%. The prognosis of ICC is poor and the 5-year survival rate in resected cases is 30 to 40% [2].

In the recent years, differences in anatomical localization as factors that could determine the prognosis of ICC has garnered attention [3, 4]. Site-specific malignancy patterns have been identified. Guedj et al. [5] reported that neuroinvasion is more frequent in perihilar ICC than in peripheral ICC (83% vs. 36%). Moreover, Lee et al. [6] demonstrated that lymph node metastasis is more common in perihilar ICC than in peripheral ICC (22.6% vs. 9.1%). These clinicopathological differences observed among ICCs suggest different origins or site effects on the process of carcinogenesis.

The hilar bile duct is formed by the union of two different embryological regions. The extrahepatic bile duct develops along with the ventral pancreas, whereas the peripheral bile duct develops from the ductal plates and periportal tissue, both of which are continuously formed by hepatoblasts. These tissues are formed together in a complex fashion in the porta hepatis, giving rise to the hilar bile duct [7-9]. This process might explain the different transcription factors detected at different sites. Anatomically, the

distinction between extrahepatic and intrahepatic bile ducts depends on anatomical landmarks. However, it has been reported that the anatomical landmark and the histological structure do not clearly coincide with each other [10]. As described above, since the perihilar region is a region where the extrahepatic bile duct and the intrahepatic bile duct join, it is suggested that the carcinogenic form in the perihilar region might differ from that in the peripheral region.

To confirm these differences, it is useful to compare perihilar type ICC and peripheral type ICC occurring simultaneously in the liver. However, ICC is a rare cancer, and it is difficult to examine human cases of ICC occurring simultaneously in two regions.

Therefore, we decided to investigate the differences between perihilar type and peripheral type ICC, using an animal model. Various methods are available to generate an animal model of ICC. One method of generating an animal model of ICC is to expose mice to carcinogens [11]; another method involves the introduction of oncogenes [12]; yet another method involves the induction of tumorigenesis in mice through xenotransplantation [13, 14]. Each of these animal models has its advantages and disadvantages. The fact that tumors formed in animal models closely resemble human ICC with respect to pathological findings and tumorigenesis pathways is significant from the viewpoint of clinical applications. The mouse model generated by Yamada et al [12]

was subjected to histopathological examination, immunocytochemistry for pancytokeratin and SOX9 expression, and analysis of changes in serum tumor markers. Furthermore, RNA sequencing has reported the close similarity in gene expression in mouse models of ICC and human ICC; in such models, multiple ICCs can be developed in the liver. Hence, this mouse model is appropriate for the present study.

We investigated these differences from two perspectives. Recent studies in this field have focused on tumor metastasis and analysis of the mechanism underlying tumor progression at the gene and protein levels.

The epithelial-mesenchymal transition (EMT) is a phenomenon in which the epithelial cells lose E-cadherin expression and gain highly motile mesenchymal properties [15], which has been shown to play a key role in the progression of various carcinomas [16-18] and might contribute to the differences observed in the clinical course of ICCs of different sites.

In 2016, the gene expression profile of biliary tract cancers was characterized, revealing 32 driver genes significantly contributing to the pathogenesis and progression of the disease [19]. Among them, EPHA2, BAP1, FGFR2, and IDH1/2 were reported as unique driver genes in ICC, and KRAS, SMAD4, ARID1A, and GNAS mutations were reported as common driver genes in both ICC and extrahepatic bile duct cancer. Oncogene

expression levels might vary by ICC site

To explore this possibility, the aim of the present study was to investigate tumor-site effects on EMT factors and driver gene expression in an ICC experimental model developing both perihilar and peripheral ICC that was previously established by Yamada et al. [12].

Materials and methods

Ethics statement

All animal experiments were approved by the animal ethics committee of Nagasaki University in accordance with the Guidelines for Animal Experimentation of Nagasaki University, and the study conformed to the recommendations in the Guide for the Care and Use of Laboratory Animals of the National Institute of Health.

Animal model

We generated a mouse model of ICC according to the previous description by Yamada et al. [11]. Male 4 - 6-week-old C57BL/6 mice were purchased from CLEA (Tokyo, Japan). Single-sex mice were used to limit variability and eliminate the possibility of sex-related

experimental confounds. The mice were anesthetized with 1.5% isoflurane, and a midline abdominal incision was made. The wound was retracted, and the liver was aligned with the diaphragm to confirm its positional anatomical relationship with the gall bladder, common bile duct, and lateral bile duct. The common bile duct was clamped with a blood vessel clip (Laboratory & Medical Supplies INS15911) and the bile duct of the left lobe was sutured with a 6 - 0 silk thread. Myristoylated-AKT1 (AKT), human YAPS127 (YAP2), and pCMV-Sleeping Beauty (SB), provided by Professor Gregory J. Gores (Liver Pathology Laboratory, Mayo Clinic), were used as the plasmids to induce tumor formation. In total, 11.25 μg of AKT, 11.25 μg of YAP 2, and 2.5 μg pCMV-SB were mixed in a suspension, and 5 μg of in vivo jet PEI (Polyplus, New York, NY, USA) was added to the mixture; 100 μL of this mixture was then injected into the gall bladder of the mice with 5% glucose solution. After injecting the turbid suspension, the gall bladder was compressed with a sterilized swab and dissected out. After a few minutes, the silk thread applied to the left lobe of the bile duct was ligated. Finally, the clip on the common bile duct was removed, and the abdominal median wound was closed with a 5 - 0 nylon thread, thereby concluding the operation. The mice were euthanized at 8, 10, 12, and 14 weeks after surgery to confirm carcinogenesis.

Hematoxylin and eosin (HE) staining

The tumors were classified into two groups according to the localization of the mass. A mass within 5 mm from the hepatic portal was defined as the perihilar type, whereas a mass located within 5 mm from the outside of the liver was defined as the peripheral type. The liver tissue was fixed with 4% paraformaldehyde (Wako Pure Chemical Industries Ltd., Osaka, Japan) for 24 h, dehydrated in increasing ethanol grades, embedded in paraffin (Paraplast Plus; Leica Biosystems Inc., Richmond, IL, USA), and cut into 5-μm-thick sections. The sections were stained with HE (Muto Pure Chemicals Co. Ltd., Tokyo, Japan). All staining procedures were performed in accordance with standard histological staining protocols.

Immunohistochemistry

The sections were deparaffinized with xylene and rehydrated in decreasing ethanol grades. After treatment with preheated pH 9.0 target retrieval solution (Agilent, Santa Clara, CA, USA), the slides were allowed to cool in water for 20 min, rinsed with phosphate-buffered saline, and soaked for 10 min at 20 °C in peroxidase-blocking solution (Agilent). The sections were incubated with the following primary antibodies at 4 °C overnight: rabbit monoclonal anti-mouse anti-cytokeratin 7 (CK7; Abcam,

Cambridge, UK), anti-CK19 (Abcam), anti-E-cadherin (Cell Signaling Technology, Tokyo, Japan), anti-vimentin (Cell Signaling Technology), anti-alpha-smooth muscle actin (α-SMA; Abcam) and neural cell adhesion molecule (NCAM; Cosmo Bio, Tokyo, Japan). After washing, the sections were treated with horseradish peroxidase-labeled goat anti-mouse and anti-rabbit immunoglobulin secondary antibodies (Agilent) at 20 °C for 30 min. Thereafter, the sections were stained with 3,3-diaminobenzidine tetrahydrochloride containing hydrogen peroxide (Agilent) and observed under a DP-74 electric inverted microscope (Olympus, Tokyo, Japan).

Reverse transcription-quantitative polymerase chain reaction (RT-qPCR) analysis

The expression levels of *Fgfr2*, *Idh1*, and *Idh2*, which have been identified as driver genes for ICC, were quantified using RT-qPCR in the two types of ICC tumors at 10 and 14 weeks. Total RNA was extracted from mouse ICC tissues using a spin column (NucleoSpin RNA II; Macherey-Nagel, Düren, Germany) in accordance with the manufacturer's instructions. The cDNA was synthesized using a high-capacity cDNA reverse transcription kit (Applied Biosystems, Tokyo, Japan) in accordance with the manufacturer's instructions. The samples were then stored at -20 °C until use. PCR was performed using an Applied Biosystems StepOnePlus Real-time PCR system with the

TaqMan Gene Expression Assay Kit (Applied Biosystems) in accordance with the manufacturer's instructions. In brief, PCR amplification was performed using a reaction mixture containing 1 μL cDNA sample, 0.5 μL TaqMan Gene Expression Assay probe, 5 μL TaqMan Fast Advanced Master Mix (Applied Biosystems), and 13.5 μL nuclease-free water. The cycling conditions were 95 °C for 1 s and 60 °C for 20 s. The comparative cycle threshold method was used to quantify relative gene expression levels normalized to those of mouse ACTB (the hepatocyte suspension was set as 1.0). The expression levels of human HIF1A and CASP3 were normalized to that of human ACTB (Fib-0.1/RH at day 1 was set as 1.0).

Western blotting

Total protein concentrations were measured using a bicinchoninic acid protein assay kit (Pierce, 23227, Thermo Fisher Scientific K.K, Tokyo, Japan) in accordance with the manufacturer's instructions. Loading buffer [50 mM Tris-HCl (pH 6.8) containing 5% glycerol, 1.6% sodium dodecyl sulfate (SDS), and 100 mM dithiothreitol] was added to the proteins, and the mixtures were incubated at 95 °C for 10 min. Proteins were separated using SDS-polyacrylamide gel electrophoresis with a 10% resolving gel. The proteins were electro-transferred onto an Immobilon-P membrane (Millipore,

IPVH10100, Sigma-Aldrich, Tokyo, Japan) in a transfer buffer containing 20% methanol, and the membrane was blocked with 5% non-fat dry milk in TBST [10 mM Tris-HCl (pH 7.8), 100 mM NaCl, 0.1% Tween 20] for 60 min at 20 °C and probed with the primary antibodies overnight at 4 °C, followed by probing with the secondary antibodies. Immunoreactive bands were visualized using the enhanced Clarity Western ECL Substrate (Bio Rad, 1705061, Tokyo, Japan). Beta-actin expression was detected before the detection of α-SMA. The membrane was then incubated with stripping buffer [6 M guanidine hydrochloride, 50 mM Tris-HCl (pH 6.8), 5% 2-mercaptoethanol] for 30 min at room temperature. The membrane was blocked and probed with the primary antibody.

Statistical analysis

The Mann–Whitney U test was used for inter-group comparisons. Multigroup comparison was examined using the Kruskal Wallis test and Steel-Dwass test. Differences were considered significant when P values were < 0.05. The Mann–Whitney U test was performed using Stat Mate V (ATMS, Tokyo, Japan). Kruskal Wallis test was performed using Ekuseru-Toukei 2015 (Social Survey Research Information, Tokyo, Japan).

Results

Comparison of immunostaining at different carcinogenesis sites

The mice were sacrificed at 8, 10, 12, and 14 weeks after injection with the plasmids and the developed tumors were examined by histopathology. Carcinogenesis was not observed in the majority of the mice sacrificed at 8 weeks. However, carcinogenesis was detected at 10 weeks after injection and was confirmed in almost all of the lobes at 14 weeks (Fig. 1a). Perihilar ICC was defined as ICC within 5 mm of the hepatic portal vein and peripheral ICC was defined as that within 5 mm of the outer edge of the liver (Fig. 1b). HE staining revealed cord-like proliferation accompanied by nuclear atypia, along with the presence of small tubular sites (Fig. 2). The cholangiocarcinoma at 10 weeks after injecting plasmids into mice was positive for CK7 and CK19 expression as bile duct markers. (Fig. 3a). The morphology of the perihilar type of ICC was irregular, whereas that of the peripheral type was circular.

Immunostaining was conducted for several cell adhesion factors and EMT factors, which revealed no difference in E-cadherin and vimentin expression between the perihilar and peripheral types (Fig. 3b). However, in α-SMA and NCAM, slight differences in immunostaining patterns between the perihilar and peripheral types were observed by microscopic observations (Fig. 3c).

Variation in protein expression according to carcinogenic sites in the ICC mouse model

The levels of proteins involved in the EMT, namely E-cadherin, vimentin, a α-SMA, and NCAM were further quantified using Western blotting (Fig. 4a and 4b). At 10 weeks, the α-SMA expression level tended to be higher in the perihilar type than that in the peripheral type ($p = 0.055$), but no significant differences were noted in the expression levels of either E-cadherin or vimentin between the two groups (Fig. 4c). At 14 weeks, vimentin expression in the perihilar type was significantly higher than that detected in the peripheral type ($p = 0.025$). However, there were no significant differences in the expression levels of the other proteins between the two ICC types (Fig. 4c). NCAM protein amount was very small and compatibility with antibody was not enough, so quantification by Western blot was not possible.

Comparison of driver genes of ICC and oncogenes

As a control, normal mouse liver tissue was used. *Fgfr2* and *Kras* of ICC were expressed at a significantly higher level than normal liver tissue in 10 weeks and 14 weeks (10weeks; *Fgfr2*: $p = 0.018$, *Kras*: $p = 0.014$, 14weeks; *Fgfr2*: $p = 0.017$, *Kras*: $p = 0.007$). The *Idh1/2* expressions of ICC were significantly lower level than normal liver tissue in

10 weeks and 14 weeks (10weeks; *Idh1*: $p = 0.007$, *Idh2*: $p = 0.017$, 14weeks; *Idh1*: $p = 0.007$, *Idh2*: $p = 0.025$). *Fgfr2* was expressed at a significantly higher level in the peripheral type of ICC at 10 weeks ($p = 0.024$), whereas the expression levels of *Idh2* were significantly higher in the perihilar type ($p = 0.042$). However, at 14 weeks, no significant difference between the groups was noted in the expression levels of *Fgfr2*, *Idh1/2*, and *Kras* (Fig. 5b)

Discussion

In this experimental model of ICC, we determined that ICC differs in terms of protein and oncogene expression depending on the carcinogenic sites, despite equal distribution of the plasmids. By utilizing an ICC mouse model, we compared the difference between purely perihilar and peripheral types of ICC. Yamashita et al. had used clinical specimens to examine the differences in the prognosis and tumor progression pattern between these two types of ICC [20]. Aishima et al. also reported the pathological differences between the two types of ICC [21]. These are especially important studies that reported the difference in the clinical course and pathology between the perihilar and peripheral types of ICC. However, comparing these two types of ICC purely on the basis of difference in the patient's age, living environment, underlying medical conditions,

cancer stage, etc. is difficult. In contrast, in our study, comparison of ICCs in mice of the same age, carcinogenetic procedures that the mice underwent, and breeding environment made it possible to rule out their nonsignificant background-related differences.

This study revealed that α-SMA expression was increased in the perihilar type at an early stage, and the expression level of vimentin subsequently increased to a significant extent in the perihilar type of ICC than in the peripheral type at 14 weeks. However, as a matter of fact, an increase in α-SMA alone may also be caused by an increase in fibroblast components, elevated vimentin and microscopic findings of cancer cell growth suggest that EMT might occur in perihilar ICC at a relatively early stage. Moreover, at 14 weeks, the perihilar type clearly exhibited characteristics of the mesenchymal system. EMT is primarily considered to play a role in the early stage of cancer development, and the relationship between EMT and cancer metastasis has attracted substantial research attention in various carcinomas [22-24]. In the recent years, microRNAs involved in EMT have also been reported as potential therapeutic targets in gastric and bladder cancers [25, 26]. Since E-cadherin, vimentin, and α-SMA are known markers for EMT [27, 28], our data suggest that the clinical course of ICC may depend on the carcinogenic site.

We further focused on the expression profiles of several driver genes that could be

therapeutic target candidates according to tumor localization. At 10 weeks after plasmid injection, the *Fgfr2* expression level was significantly higher in the peripheral type than in the perihilar type, whereas *Idh2* expression levels exhibited the opposite pattern. This finding suggests that the expression of these driver genes varies depending on tumor localization. Interestingly, there was no significant difference in driver gene expression at 14 weeks after carcinogenesis initiation, indicating that their expression levels fluctuate depending on the stage of cancer progression.

These site-specific patterns can provide new insights into the development of targeted therapy in ICC. For unresectable ICCs, gemcitabine / cisplatin therapy, and tegafur, gimeracil, and oteracil potassium are typically used as chemotherapy agents; however, these treatments are not sufficiently effective. To improve treatment outcomes with chemotherapy, genetic analysis of the ICC tumor will be important for an appropriate selection of chemotherapy and molecular-targeted therapeutic agents. The timing of therapeutic intervention may also be an important consideration in achieving a good therapeutic effect. Although the development of molecular therapeutic agents targeting FGFR2 (Infigratinib) for biliary tract cancer has attracted substantial attention in recent years [29, 30], our results suggest that these agents would be more effective in peripheral ICC than in perihilar ICC from early stage. In addition, although there is no difference

in expression at 14 weeks, the expression is significantly higher than in normal cells, suggesting that FGFR2 may be a therapeutic target in ICC in all regions. To confirm this possibility, *in vivo* dosing experiments are needed to evaluate any difference in treatment efficacy depending on the timing of therapeutic intervention.

This study faced some limitations. First, the carcinogenic process is dependent on the plasmids. Carcinogenesis induced using plasmids is different from that observed in actual clinical practice. In this mouse model, carcinogenesis is induced by a plasmid randomly incorporated into the bile duct epithelium from the reagent. The background of carcinogenesis varies depending on the carcinogenic site; thus, considering the background of carcinogenesis is also important [6]. However, it is a key point that attention can be paid to only the site of the carcinomatous bile duct by making the carcinogenesis mechanism uniform. Second, perihilar type ICC clinicopathologically has a stronger tendency to invade the nerve than peripheral type ICC. EMT theory strongly correlates with cancer metastasis but not with neuroinvasive tendency. Immunostaining and Western blotting to prove the difference in neural invasion tendency were performed using NCAM as a marker used for indicating nerve infiltration. Immunostaining appeared to be slightly more expressed in the perihilar type than peripheral type, but quantitative comparison was difficult because of low protein expression. Third,

comparing the prognosis of perihilar type ICC with peripheral type ICC was difficult in our study because ICC occurs frequently in the liver. However, in our study, we clarified the difference in the therapeutic oncogene expression patterns in these two types of ICC. Fourth, the differences in genes expression levels were clarified, but the degree of mutation in each genes were not examined. As for *Idh1/2,* the ratio of mutant *Idh1/2* increased as canceration progresses. Mutant *Idh1/2* were not amplified by wild-type *Idh1/2* primers, and its expression is considered to be lower than that of normal tissues in ICC group. For more accurate examination, the mutation rate of each gene should be examined. However, what is important in this study is to clarify the difference in gene expression at the site of carcinogenesis. It is necessary to examine the gene mutation rate in order to assist in the selection of chemotherapy in the future.

Conclusions

The microenvironment of the tumor likely influences driver gene expression in ICC and causes diverse effects on the EMT in early carcinogenesis. Such site-dependent effects could explain the observed differences in the clinical course of perihilar and peripheral ICC. Further elucidation of the expression patterns and timing of driver genes will be valuable for guiding the selection of appropriate drugs in the molecular-targeted therapy

for ICC.

Disclosure statement

Authors declare no conflicts of interest for this article.

References

1. Liver Cancer Study Group of Japan. Primary liver cancer in Japan. Clinicopathologic features and results of surgical treatment. Ann Surg 1990;211:277–87.

2. Nakagohri T, Kinoshita T, Konishi M, Takahashi S, Gotohda N. Surgical Outcome and Prognostic Factors in Intrahepatic Cholangiocarcinoma. World J Surg 2008;32:2675–80. https://doi.org/10.1007/s00268-008-9778-3.

3. Waseem D, Patel T. Intrahepatic, Perihilar and Distal Cholangiocarcinoma: Management and Outcomes. Ann Hepatol 2017;16:133–9.

4. Zhang X-F, Bagante F, Chen Q, Beal EW, Lv Y, Weiss M, et al. Perioperative and long-term outcome of intrahepatic cholangiocarcinoma involving the hepatic hilus after curative-intent resection: comparison with peripheral intrahepatic cholangiocarcinoma and hilar cholangiocarcinoma. Surgery 2018;163:1114–20. https://doi.org/10.1016/j.surg.2018.01.001.

5. Guedj N, Zhan Q, Perigny M, Rautou P-E, Degos F, Belghiti J, et al. Comparative protein expression profiles of hilar and peripheral hepatic cholangiocarcinomas. Journal of Hepatology 2009;51:93–101. https://doi.org/10.1016/j.jhep.2009.03.017.

6. Lee H, Wang K, Johnson A, Jones DM, Ali SM, Elvin JA, et al. Comprehensive

genomic profiling of extrahepatic cholangiocarcinoma reveals a long tail of therapeutic targets. J Clin Pathol 2016;69:403–8. https://doi.org/10.1136/jclinpath-2015-203394.

7. Van Eyken P, Sciot R, Callea F, Steen KVD, Moerman P, Desmet VJ. The development of the intrahepatic bile ducts in man: A keratin-immunohistochemical study. Hepatology 1988;8:1586–95. https://doi.org/10.1002/hep.1840080619.

8. Tan CEL, Vijayan V. New clues for the developing human biliary system at the porta hepatis. Journal of Hepato-Biliary-Pancreatic Surgery 2001;8:295–302. https://doi.org/10.1007/s005340170001.

9. Roskams T, Desmet V. Embryology of Extra- and Intrahepatic Bile Ducts, the Ductal plate. Anat Rec 2008;291:628–35. https://doi.org/10.1002/ar.20710.

10. Kikuchi Y, Matuyama R, Hiroshima Y, Murakami T, Morioka D, Endo I, et al. Surgical and histological boundary of the hepatic hilar plate system: basic study relevant to surgery for hilar cholangiocarcinoma regarding the “true” proximal ductal margin. Journal of Hepato-Biliary-Pancreatic Science 2019;26:159-68. https://doi.org/10.1002/jhbp.617

11. Tajima Y, Tomioka T, Ikematsu Y, Yamanaka S, Kuroki T, Kitajima T, et al.

Experimental study on pathogenesis and histomorphology of early carcinoma of the extrahepatic bile duct in the Syrian hamster. J Exp Clin Cancer Res 2005;24:475–82.

12. Yamada D, Rizvi S, Razumilava N, Bronk SF, Davila JI, Champion MD, et al. IL-33 facilitates oncogene-induced cholangiocarcinoma in mice by an interleukin-6-sensitive mechanism: HEPATOBILIARY MALIGNANCIES. Hepatology 2015;61:1627–42. https://doi.org/10.1002/hep.27687.

13. Martínez AK, Jensen K, Hall C, O'Brien A, Ehrlich L, White T, et al. Nicotine Promotes Cholangiocarcinoma Growth in Xenograft Mice. The American Journal of Pathology 2017;187:1093–105. https://doi.org/10.1016/j.ajpath.2017.01.011.

14. Vaeteewoottacharn K, Pairojkul C, Kariya R, Muisuk K, Imtawil K, Chamgramol Y, et al. Establishment of Highly Transplantable Cholangiocarcinoma Cell Lines from a Patient-Derived Xenograft Mouse Model. Cells 2019;8:496. https://doi.org/10.3390/cells8050496.

15. Hay ED. The mesenchymal cell, its role in the embryo, and the remarkable signaling mechanisms that create it. Dev Dyn 2005;233:706–20. https://doi.org/10.1002/dvdy.20345.

16. Chen G, Zhou T, Ma T, Cao T, Yu Z. Oncogenic effect of PHLDB2 is associated with

epithelial–mesenchymal transition and E-cadherin regulation in colorectal cancer. Cancer Cell Int 2019;19:184. https://doi.org/10.1186/s12935-019-0903-1.

17. Das K, Paul S, Singh A, Ghosh A, Roy A, Ansari SA, et al. Triple-negative breast cancer-derived microvesicles transfer microRNA221 to the recipient cells and thereby promote epithelial-to-mesenchymal transition. J Biol Chem 2019;294:13681–96. https://doi.org/10.1074/jbc.RA119.008619.

18. Wang H, Zhan M, Liu Q, Wang J. Glycochenodeoxycholate promotes the metastasis of gallbladder cancer cells by inducing epithelial to mesenchymal transition via activation of SOCS3/JAK2/STAT3 signaling pathway. Journal of Cellular Physiology 2020;235:1615–23. https://doi.org/10.1002/jcp.29080.

19. Nakamura H, Arai Y, Totoki Y, Shirota T, Elzawahry A, Kato M, et al. Genomic spectra of biliary tract cancer. Nat Genet 2015;47:1003–10. https://doi.org/10.1038/ng.3375.

20. Yamashita Y-I, Wang H, Kurihara T, Tsujita E, Nishie A, Imai K, et al. Clinical Significances of Preoperative Classification of Intrahepatic Cholangiocarcinoma: Different Characteristics of Perihilar vs. Peripheral ICC. AR 2016;36:6563–70. https://doi.org/10.21873/anticanres.11260.

21. Aishima S, Oda Y. Pathogenesis and classification of intrahepatic

cholangiocarcinoma: different characters of perihilar large duct type versus peripheral small duct type. J Hepatobiliary Pancreat Sci 2015;22:94–100. https://doi.org/10.1002/jhbp.154.

22. Labelle M, Begum S, Hynes RO. Direct Signaling between Platelets and Cancer Cells Induces an Epithelial-Mesenchymal-Like Transition and Promotes Metastasis. Cancer Cell 2011;20:576–90. https://doi.org/10.1016/j.ccr.2011.09.009.

23. Franchi M, Masola V, Bellin G, Onisto M, Karamanos K-A, Piperigkou Z. Collagen Fiber Array of Peritumoral Stroma Influences Epithelial-to-Mesenchymal Transition and Invasive Potential of Mammary Cancer Cells. JCM 2019;8:213. https://doi.org/10.3390/jcm8020213.

24. Zada S, Hwang J, Ahmed M, Lai T, Pham T, Kim D. Control of the Epithelial-to-Mesenchymal Transition and Cancer Metastasis by Autophagy-Dependent SNAI1 Degradation. Cells 2019;8:129. https://doi.org/10.3390/cells8020129.

25. Yang Y-J, Luo S, Wang L-S. Effects of microRNA-378 on epithelial-mesenchymal transition, migration, invasion and prognosis in gastric carcinoma by targeting BMP2. Eur Rev Med Pharmacol Sci 2019;23:5176–86. https://doi.org/10.26355/eurrev_201906_18182.

26. Yan T, Ye X-X. MicroRNA-328-3p inhibits the tumorigenesis of bladder cancer

through targeting ITGA5 and inactivating PI3K/AKT pathway. Eur Rev Med Pharmacol Sci 2019;23:5139–48. https://doi.org/10.26355/eurrev_201906_18178.

27. Lamouille S, Xu J, Derynck R. Molecular mechanisms of epithelial–mesenchymal transition. Nat Rev Mol Cell Biol 2014;15:178–96. https://doi.org/10.1038/nrm3758.

28. Yeung KT, Yang J. Epithelial-mesenchymal transition in tumor metastasis. Mol Oncol 2017;11:28–39. https://doi.org/10.1002/1878-0261.12017.

29. Mahipal A, Tella SH, Kommalapati A, Anaya D, Kim R. FGFR2 genomic aberrations: Achilles heel in the management of advanced cholangiocarcinoma. Cancer Treatment Reviews 2019;78:1–7. https://doi.org/10.1016/j.ctrv.2019.06.003.

30. Krook MA, Lenyo A, Wilberding M, Barker H, Dantuono M, Bailey KM, et al. Efficacy of FGFR inhibitors and combination therapies for acquired resistance in FGFR2-fusion cholangiocarcinoma. Mol Cancer Ther 2020. https://doi.org/10.1158/1535-7163.MCT-19-0631.

Figure legends

Fig. 1. (a) Morphological changes in the liver after plasmid injection. At 8 weeks, most of the mice did not develop cancer. Tumorigenesis was observed after 10 weeks, and tumor detection was more frequent over time, along with an increase in the tumor diameter. (b) The tumors in the liver were divided into two types: perihilar and peripheral. Perihilar ICC was defined as ICC within 5 mm of the hepatic portal and peripheral ICC was defined as ICC within 5 mm of the outer edge of the liver.

Fig. 2. HE staining of the ICC samples at 10 weeks after plasmid injection. HE staining revealed cord-like proliferation accompanied by nuclear atypia, along with the presence of small tubular sites. There was no significant difference between the perihilar type and peripheral type.

Fig. 3. Comparison of mice at 10 weeks after plasmid injection. (a) Immunostaining of CK7 and CK19, markers of bile duct components. Both peripheral and perihilar ICC tumors expressed these markers, with no differences between the two groups. (b) In both groups, E-cadherin, an important cell adhesion factor, was expressed on the cell membrane, with no difference between the groups. In addition, no significant difference

was observed in the expression levels of vimentin, an important marker of the EMT, between the two groups. (c) The expression levels of α-SMA, another marker of EMT, was highly increased in the perihilar type, suggesting the acquisition of mesenchymal traits. NCAM as a marker for nerve invasion is frequently expressed in the perihilar type. This suggests that perihilar ICC might have a higher tendency to infiltrate.

Fig. 4. (a, b) Comparison of protein expression in peripheral and perihilar ICC tumors at 10 and 14 weeks after injection performed using Western blotting; ACTB was used as a loading control. (c) Quantification of the expression levels of α-SMA, E-cadherin, vimentin, and other proteins in the two ICC types at 10 and 14 weeks. In mice, at 10 weeks after injection, αSMA was highly expressed in the perihilar type ($p = 0.055$). There was no significant difference in the expression patterns of other proteins between these two types of ICC. In mice, at 14 weeks after injection, vimintin expression was significantly increased in the perihilar type ($p = 0.025$). The expression of no other protein was significant. NCAM could not be quantified because the amount of protein was very small and the reaction with the antibody was poor.

Error bars represent maximum and minimum values. N.S. = not significant; $*p < 0.05$.

Fig. 5. Relative expression levels of driver genes in the two types of ICC at (a) 10 and (b) 14 weeks after plasmid injection. As a control, normal mouse liver tissue was used and quantified by quantitative reverse transcription polymerase chain reaction on the same plate (n = 3). In the 10-week-old mice (n = 5), *Idh2* were significantly expressed in the perihilar type of ICC ($p = 0.042$). In contrast, *Fgfr2* was significantly expressed in the peripheral type of ICC ($p = 0.024$). No significant difference in oncogene expression was observed in the 14-week-old mice (n = 5).

Error bars represent maximum and minimum values. N.S. = not significant; *$p < 0.05$

Fig 1a Carcinogenesis in the mouse liver

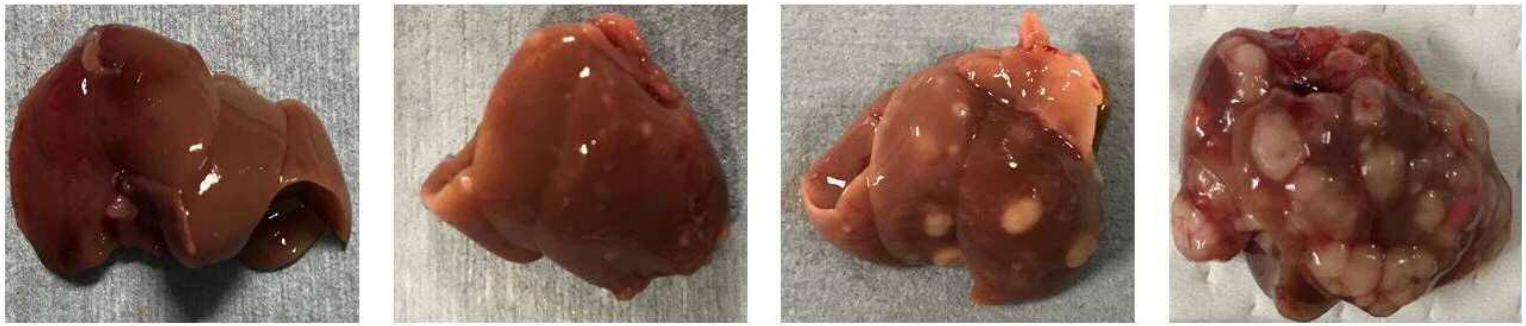

8 weeks 10 weeks 12 weeks 14 weeks

Time elapsed after plasmid injection

Fig 1b Image depicting the perihilar and peripheral types of intrahepatic cholangiocarcinoma

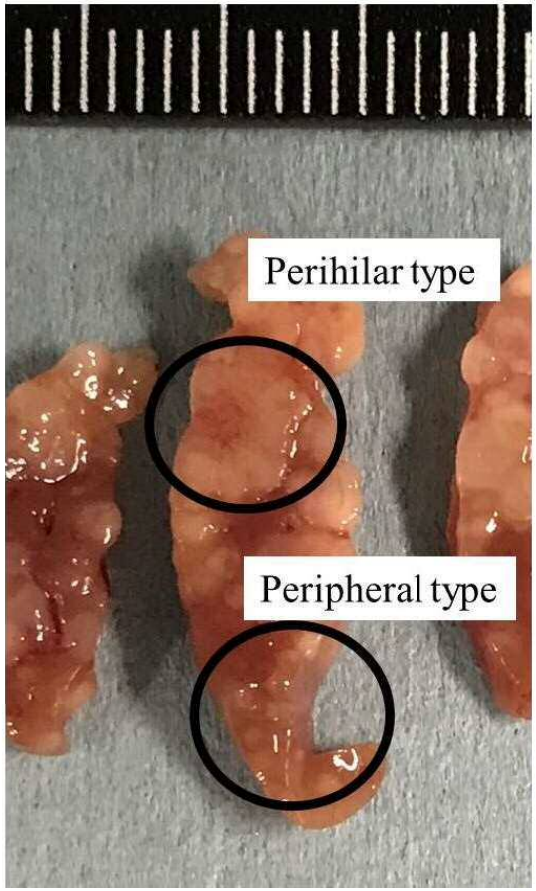

Fig 2 Immunostaining of intrahepatic cholangiocarcinoma (HE)

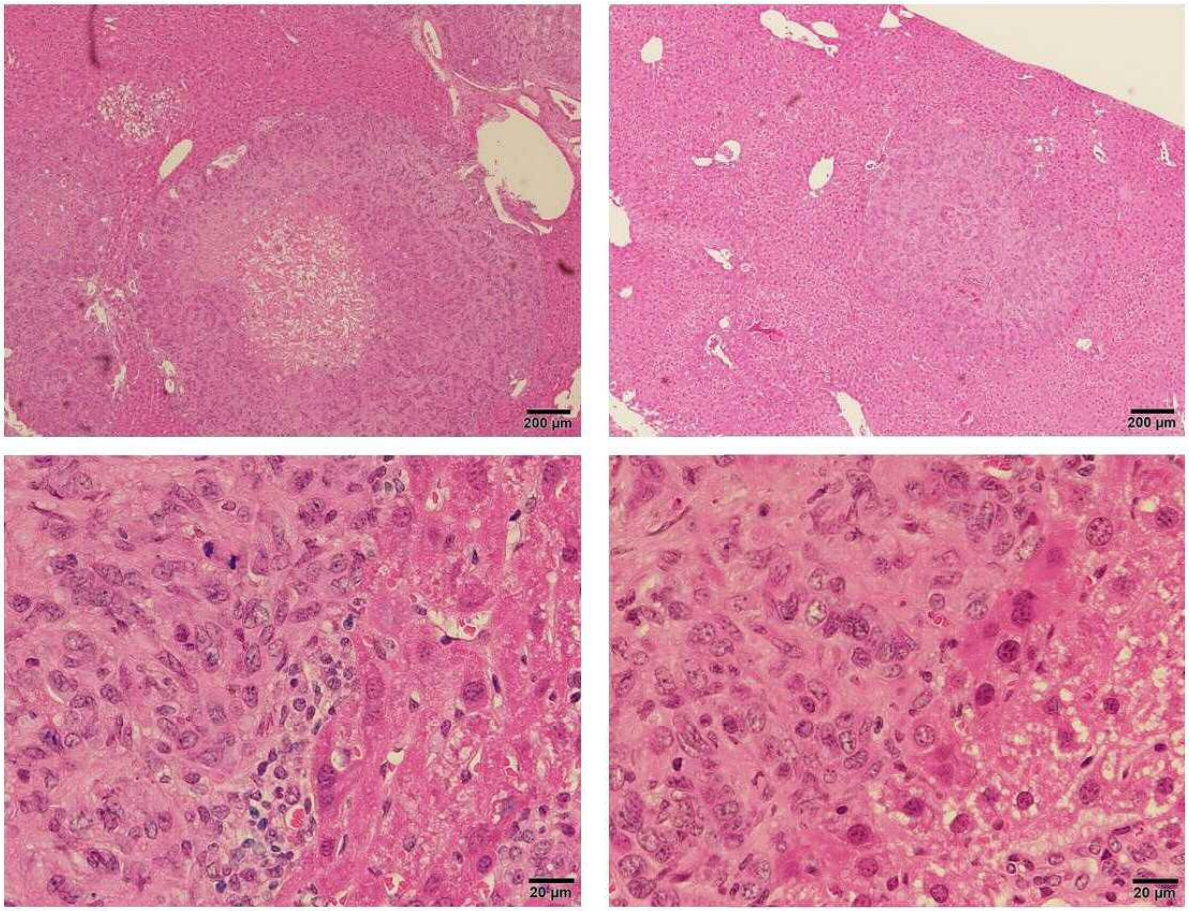

Perihilar type

Peripheral type

Fig 3a

Immunostaining of CK7 and CK19 in intrahepatic cholangiocarcinoma

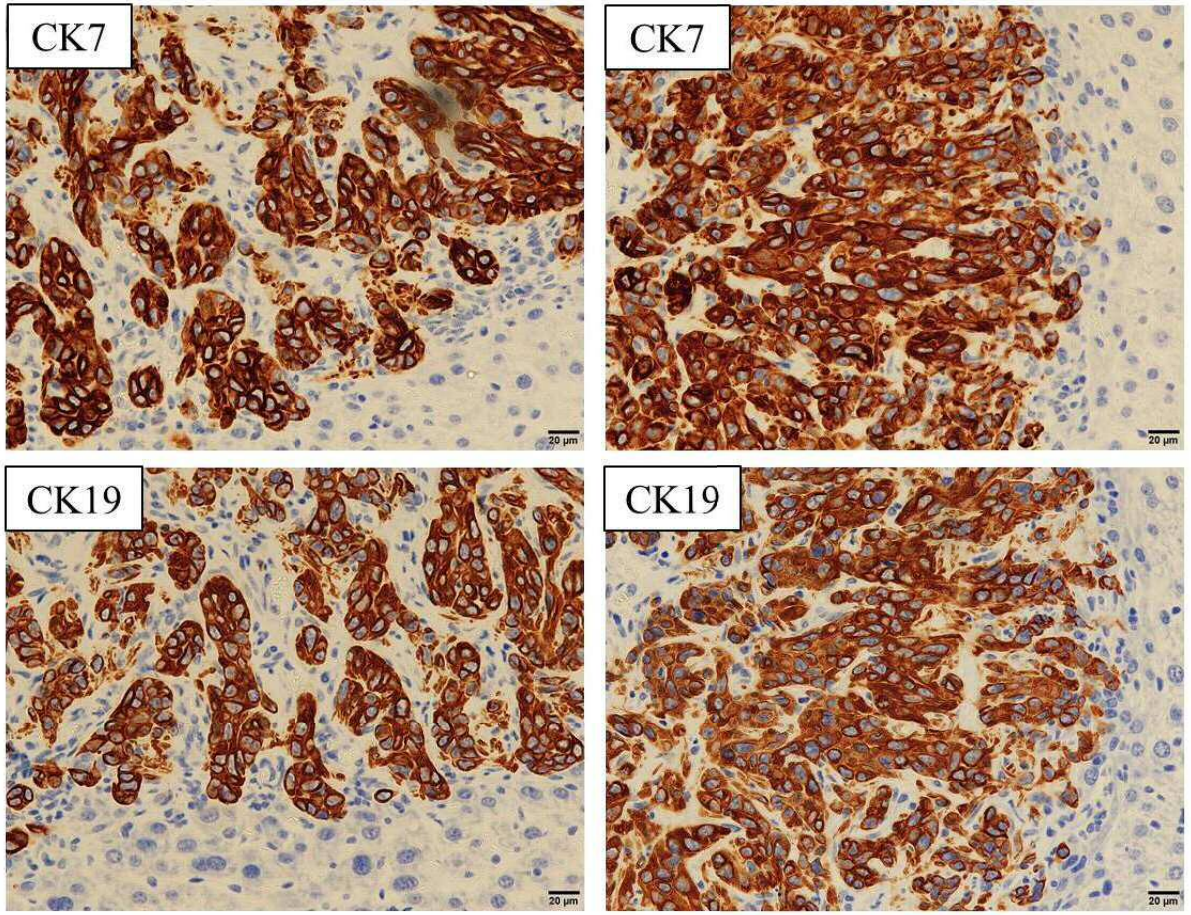

Perihilar type

Peripheral type

Fig 3b Immunostaining of E-cadherin and vimentin in intrahepatic cholangiocarcinoma

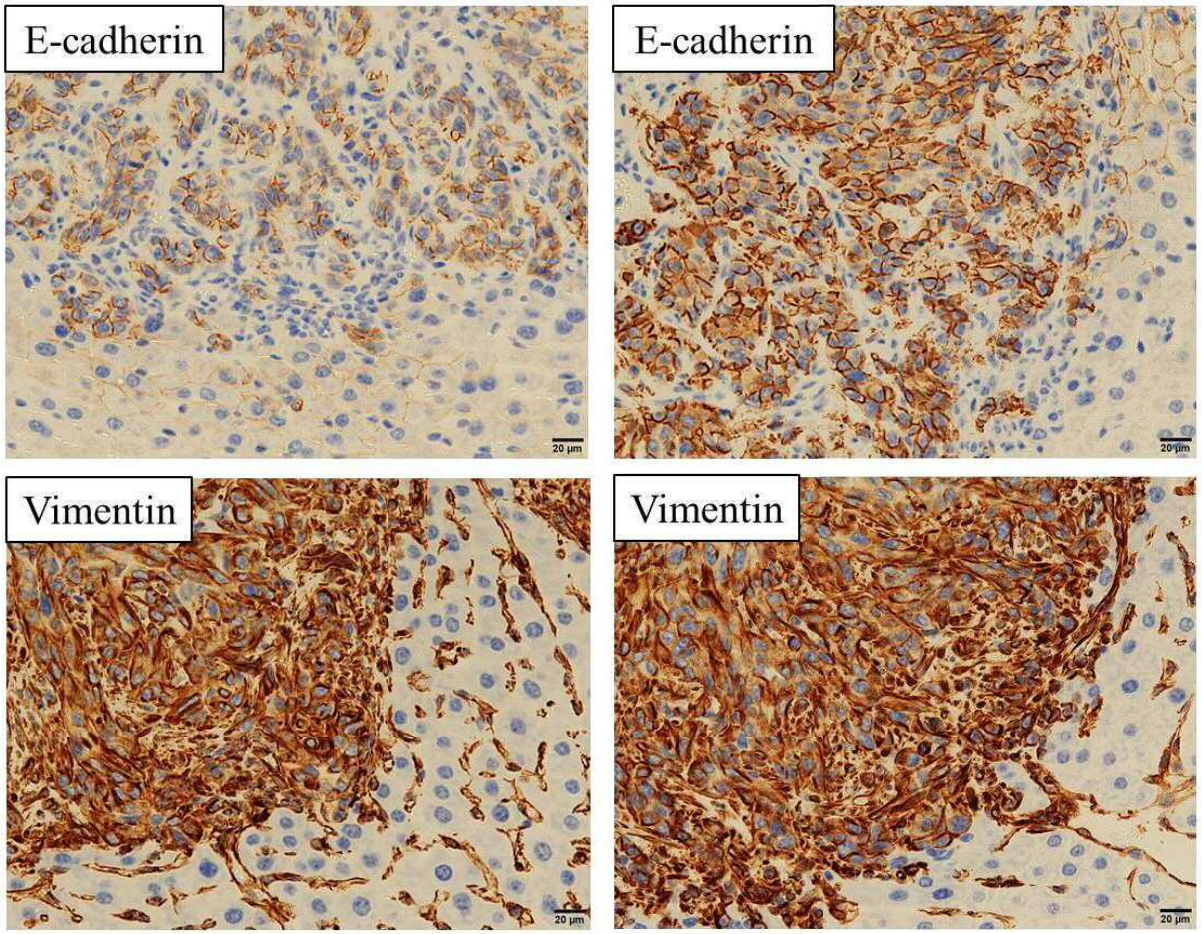

Perihilar type

Peripheral type

Fig 3c Immunostaining of α-SMA and NCAM in intrahepatic cholangiocarcinoma

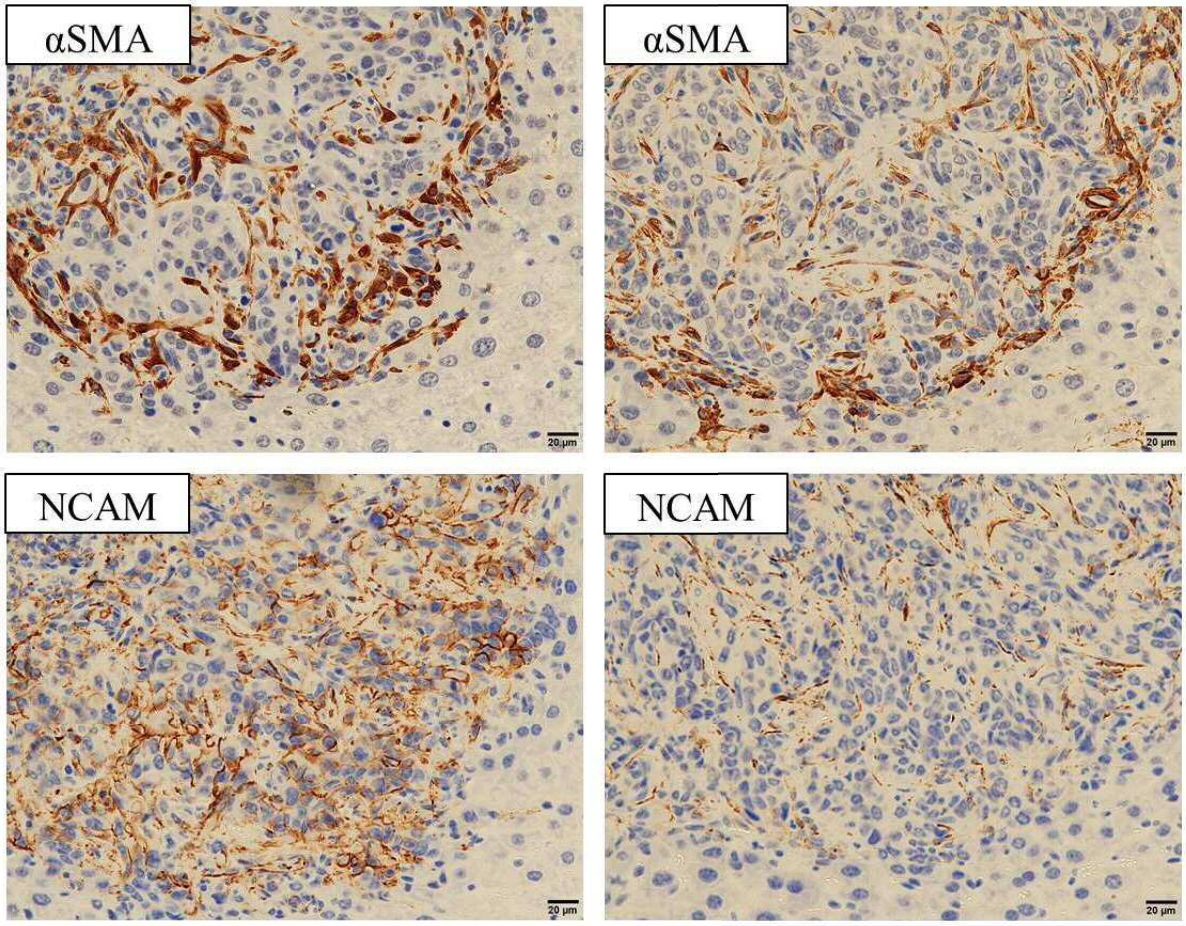

Perihilar type Peripheral type

Fig 4a Protein expression in ICC samples at 10 weeks after plasmid injection

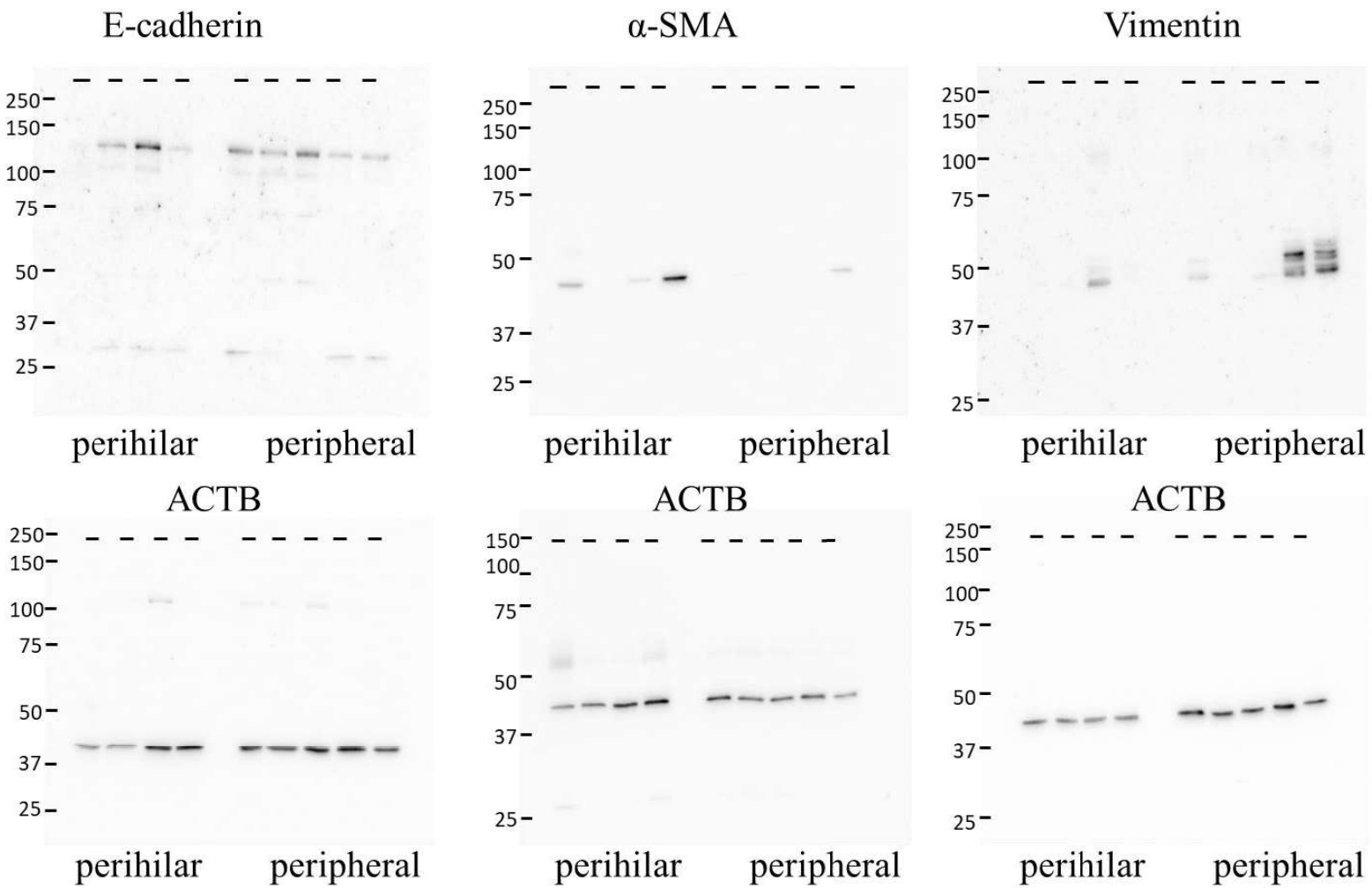

Fig 4b Protein expression in ICC samples at 14 weeks after plasmid injection

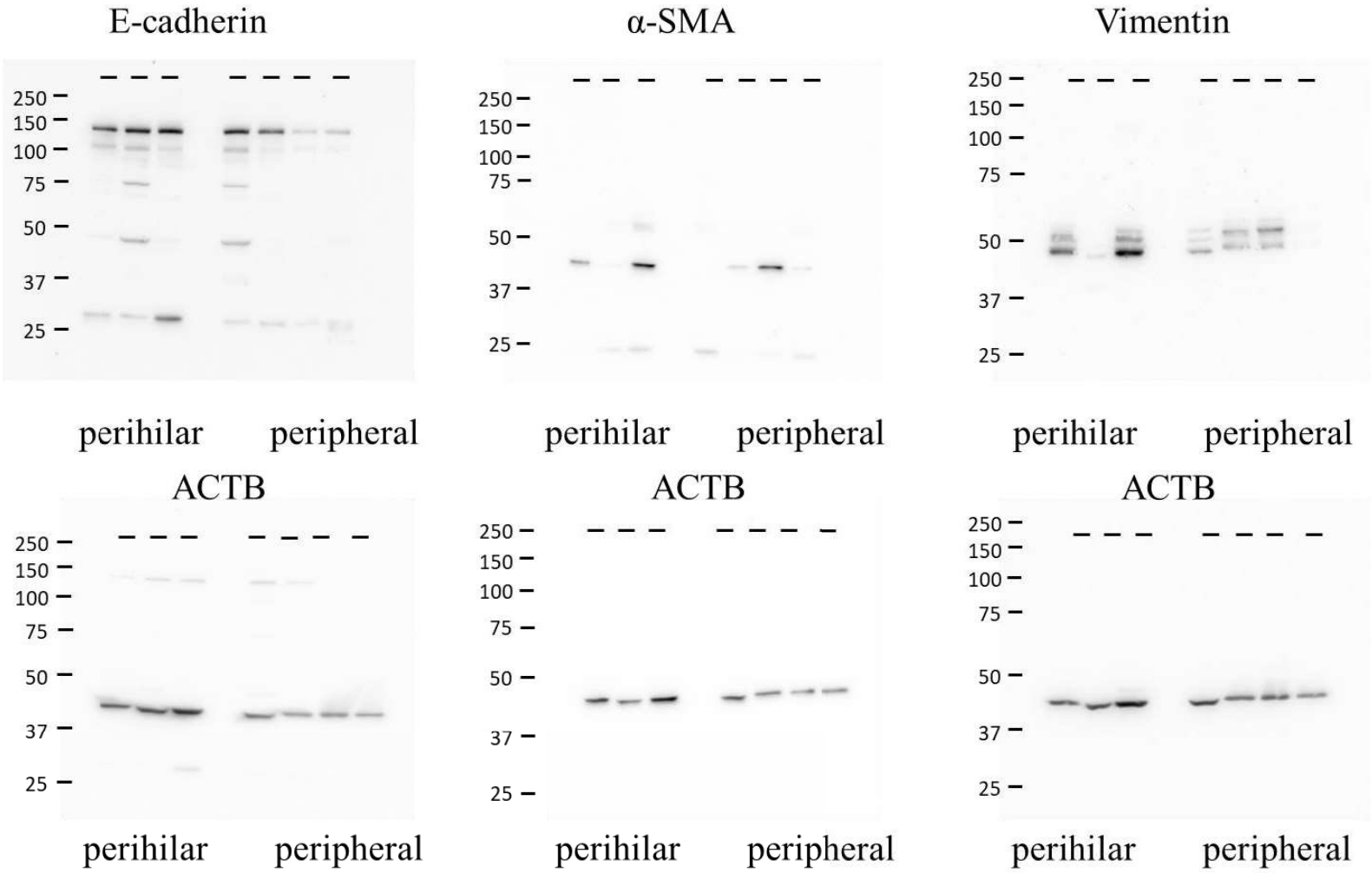

Fig 4c

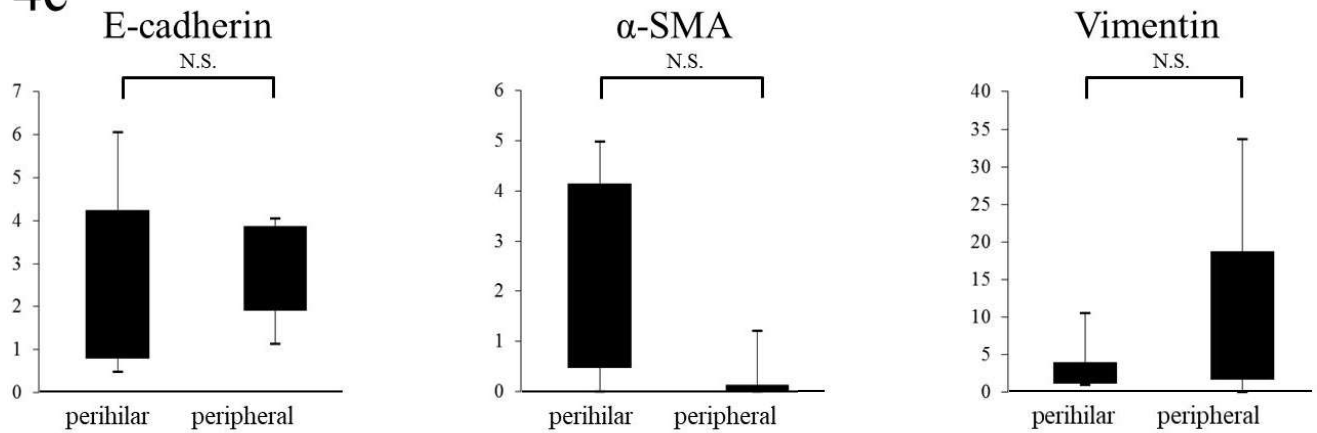

protein expression levels in intrahepatic cholangiocarcinoma at 10 weeks after plasmid injection

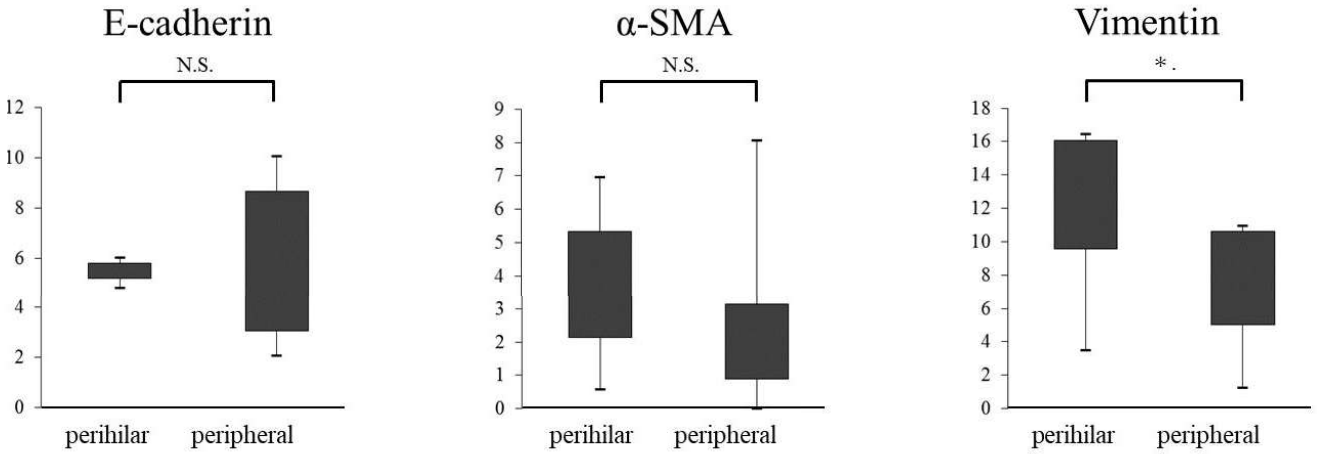

protein expression levels in intrahepatic cholangiocarcinoma at 14 weeks after plasmid injection

Fig 5a

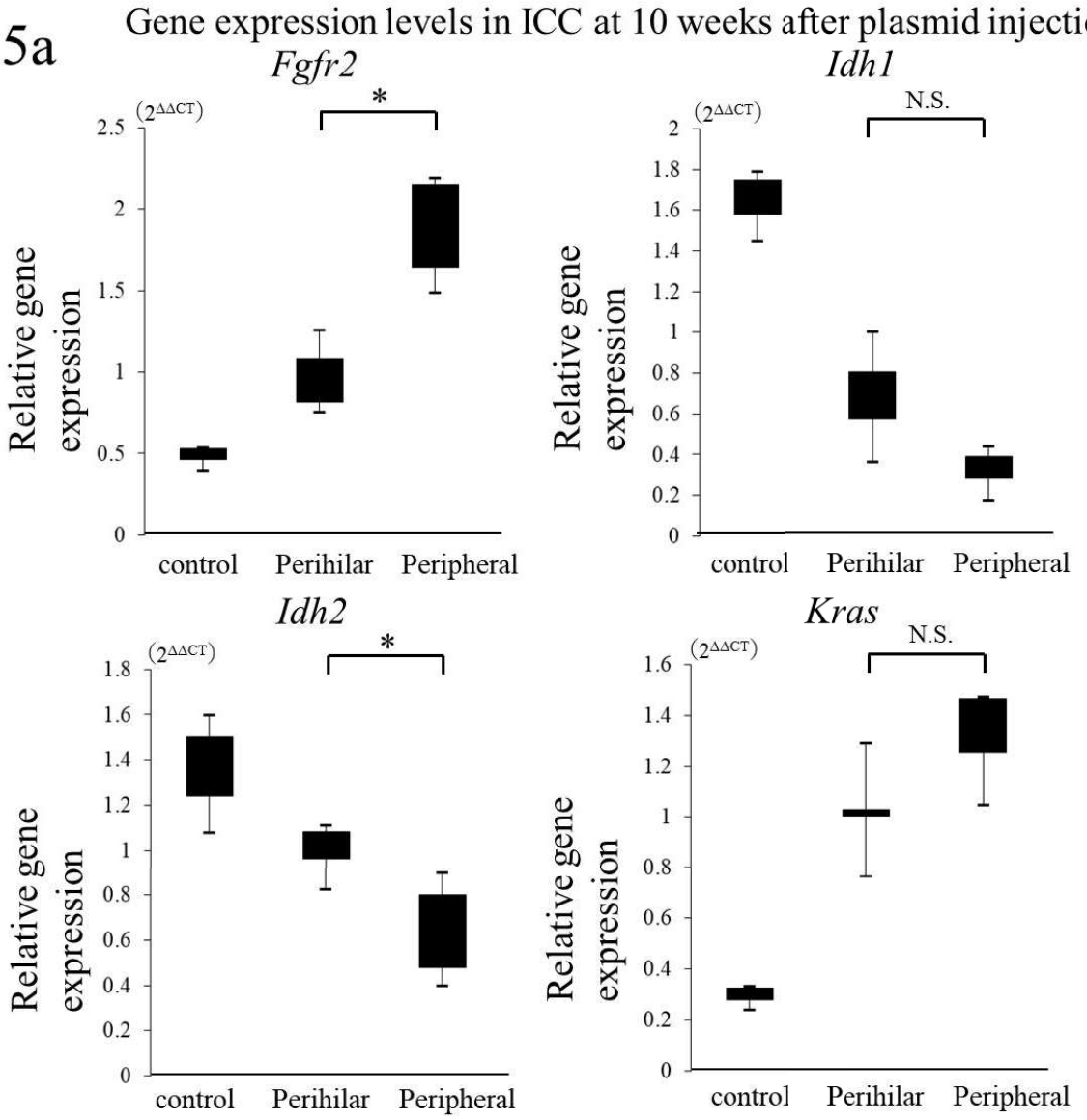
Gene expression levels in ICC at 10 weeks after plasmid injection
Fgfr2
Idh1
Idh2
Kras
Relative gene expression
(2^ΔΔCT)
*
N.S.
control
Perihilar
Peripheral

Fig 5b

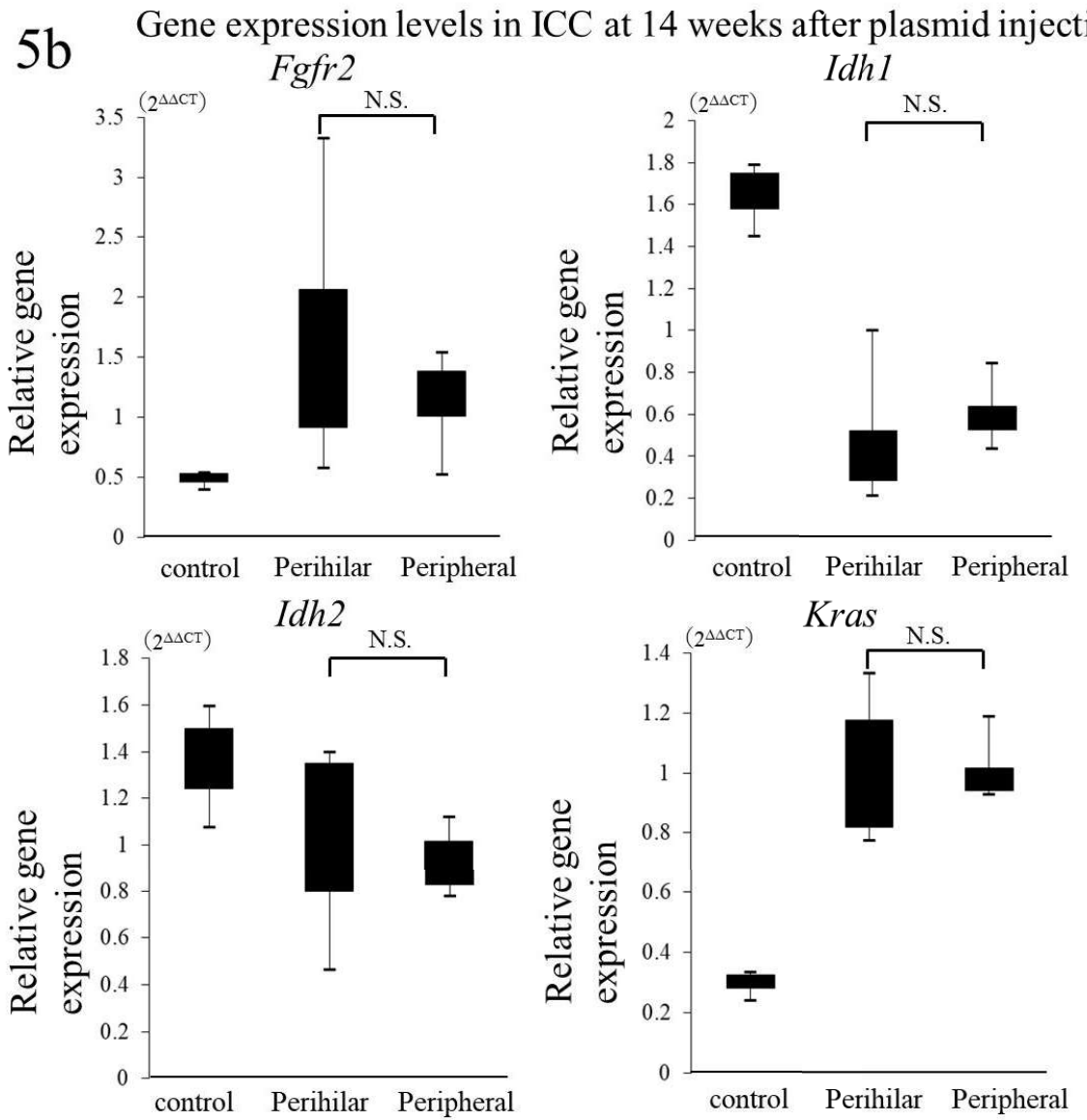
Gene expression levels in ICC at 14 weeks after plasmid injection
Fgfr2
Idh1
Idh2
Kras
(2^-ΔΔCT)
N.S.
Relative gene expression
control
Perihilar
Peripheral